22

UGVA-DPNC 1996/8-168
UT-ICEPP 96-02

FERMILAB
OCT 2 1996
LIBRARY

UGVA-DPNC-1996-8-168

Beam Energy Measurement at LEP2 Using Møller Scattering

C.Cecchi[1], **J.H.Field** [2]

Département de Physique Nucléaire et Corpusculaire Université de Genève . 24, quai Ernest-Ansermet CH-1211 Genève 4.

T.Kawamoto [3]

International Center for Elementary Particle Physics, University of Tokyo, 7-3-1 Hongo, Bunkyo-ku, Tokyo 113, Japan

Fermilab Library
0 1160 0066944 4

Abstract

A detailed study has been made of the feasibility of Møller Scattering as a method for continuous monitoring of the LEP beam energy at high energies where the currently used resonant depolarisation technique may be unusable. Two methods, based on Møller Scattering, to measure the energy with different dominant systematic errors are discussed. Monte Carlo studies of the effect on the energy measurement of radiative corrections, target binding effects, beam parameters and calorimetric energy resolution have been made. It is shown how the beam parameters necessary to control the systematic error may be deduced from the Møller scattering events, and the crucial target-detector distance monitored using ep scattering events. The beam energy precision is expected to be a few MeV at 90 GeV. The reduction of the systematic error on the W mass measurement can be appreciable, and for a fixed total error on the W mass may provide a considerable economy in running time at LEP2. The method is also applicable to precise energy measurement at high energy electron linear colliders.

NAME
ID. #
M.S.
FERMILAB LIBRARY

[1] E-mail claudia.cecchi@cern.ch
[2] E-mail john.field@cern.ch
[3] E-mail tatsuo.kawamoto@cern.ch

1 Introduction

At LEP1 with collision energies $\simeq$ 90 GeV the beam energy has been measured with a precision $\simeq$ 1 MeV [1] using the Resonant Depolarisation (RDP) method [2]. RDP at LEP1 relies on the existence of transverse polarisation in single circulating beams generated by the Sokolov-Ternov [3] mechanism. At LEP2 with collision energies $\simeq$ 200 GeV it is however not clear that the RDP method will be applicable. This is because the beam energy spread of 150 MeV at $E_{\rm beam}$ = 90 GeV (as compared to 37 MeV at $E_{\rm beam}$ = 45 GeV) is comparable to the separation of 440 MeV between adjacent linear depolarising resonances. In the absence of RDP measurements of $E_{\rm beam}$ around 90 GeV it has been proposed to use RDP up to the highest possible energy (perhaps $E_{\rm beam}$ = 70 GeV) and then to extrapolate to higher energies with the flux loop [4] method. The precision obtained in this way will depend critically on the highest energy at which RDP may be used. The error on $E_{\rm beam}$ has been estimated [4] to be in the range 9-20 MeV.

The beam energy uncertainty $\Delta E_{\rm beam}$ has a major impact on the precision of the W mass measurement at LEP2. The systematic error due to theoretical and detector based uncertainties, ΔM_W^{TD}, has been estimated to be 24 MeV [5] . With an integrated luminosity of 500 pb^{-1} per experiment, the combined statistical error on $M_{\rm W}$ of the four LEP experiments is expected [5] to be 25 MeV. Using the flux loop extrapolation method, the systematic errors on $M_{\rm W}$ from $\Delta E_{\rm beam}$, (ΔM_W^E) and from theoretical and detector related uncertainties (ΔM_W^{TD}) are comparable, [4] and the combined systematic error on $M_{\rm W}$ is expected to be greater than, or of the order of, the statistical one. If a dramatic improvement, (say by a factor of 5) in $\Delta E_{\rm beam}$ is possible its contribution to the systematic error on M_W will be negligible. It may also be remarked that theory and detector related systematic errors of physical observables estimated in early LEP1 studies have, in some cases, been shown in practice to be pessimistic by an order of magnitude or more. The impact of $\Delta E_{\rm beam}$ on the total error on the W mass and the required integrated luminosity at LEP2 is considered in more detail in Section 5 below.

One possibility to reduce significantly $\Delta E_{\rm beam}$ (to the level of 2 MeV at $E_{\rm beam}$ = 90 GeV) is the Møller scattering technique [6, 4]. This possibility is explored in detail in this paper. It is proposed to cross-calibrate with RDP at any convenient low energy (say $E_{\rm beam}$ = 50 GeV) and to use the Møller technique at all higher energies. It is important to note that, unlike RDP, the Møller method gives a continuous measurement of the electron beam energy with colliding beams in the machine, thus avoiding the time dependent interpolation errors of the RDP method [5]. Since the energy is measured at a unique point in the machine an extrapolation to the corresponding energies in the four experimental interaction regions is however required. Also in the RDP method the measured energy (the average over the circumference) must be similarly extrapolated. By use of a symmetric detector it is, in principle, also possible to measure the energy of the e^+ beam, using Bhabha scattering. However space limitation in LEP may preclude this possibility.

The plan of the paper is as follows: in Section 2 the basic method is explained and the critical parameters contributing to $\Delta E_{\rm beam}$ are introduced. In Section 3 results from Monte Carlo

[4] Note that $\Delta E_{\rm beam} = \Delta M_W^E$.

[5] In fact these give the main contribution to $\Delta E_{\rm beam}$ for the RDP method. The intrinsic accuracy (resonant line width) is only $\simeq$ 250 keV at LEP1 [7].

simulations of the detector are presented. Effects considered include calorimeter resolution and gain stability, QED radiative corrections, target binding effects and finite beam size and angular divergence. Section 4 is devoted to calibration procedures. It turns out that all essential parameters, except the target-detector distance, are measurable using only the recorded Møller scattering events. Detecting also elastic ep scattering events enables precise monitoring the target-detector distance. The conclusions are presented in Section 5.

2 Basic Method

We consider elastic scattering of a beam electron (or positron) of energy $E_{\rm beam}$ on a target electron at rest. From two body kinematics we have the relation [6] :

$$E_{\rm beam} = \frac{8m_e}{\theta_0^2} \cdot \frac{1}{1-\kappa^2} - m_e \tag{1}$$

where m_e is the electron mass and θ_0 is the 'opening angle' between the two scattered electrons in the lab. frame defined by:

$$\theta_0 \equiv \tan\theta_1 + \tan\theta_2. \tag{2}$$

here θ_1 and θ_2 are the scattering angles of the two electrons with respect to the beam direction. The parameter κ is the cosine of the scattering angle of the electron in the centre of mass system ($\kappa = \cos\theta^*$), which can be determined using the quantities in the laboratory system by either:

$$\kappa = \frac{\tan\theta_1 - \tan\theta_2}{\tan\theta_1 + \tan\theta_2} \tag{3}$$

or

$$\kappa = \frac{E_{\rm beam} + m_e}{E_{\rm beam} - m_e} \cdot \frac{E_1 - E_2}{E_1 + E_2} \simeq \frac{E_1 - E_2}{E_1 + E_2} \tag{4}$$

here E_1, E_2 are the energies of the scattered electrons. The principle of the Møller technique is to measure θ_0 and κ, and determine the $E_{\rm beam}$ using Eqn.(1). At $E_{\rm beam} = 90$ GeV, the minimum opening angle (for $\kappa = 0$) is 6.74 mrad.

The proposed detector is shown schematically in figure 1. It consists of the following elements:

- A hydrogen gas jet target (GJT) similar to that used in the UA6 experiment [8]. The bound electrons of the hydrogen atoms serve as target.
- A silicon microstrip detector (SMD) with full azimuthal acceptance and a polar angle acceptance from 2 to 10 mrad measuring (r, ϕ) co-ordinates in a plane transverse to the beams.

[6] A slightly different formula is given in Ref.[6]. It differs from Eqn.(1) only by terms of $O((\frac{m_e}{E_{\rm beam}})^2)$

- A high resolution electromagnetic calorimeter (ECAL) with a similar angular coverage to the SMD.
- A recoil proton detector (RPD) consisting of a small planar silicon microstrip detector *in vacuo* close to the GJT, to detect recoil protons from elastic e-p scattering.

As indicated in figure 1 the scattered electrons are detected in a near-symmetric configuration where each has an energy of $\simeq E_{\rm beam}/2$ and $\theta_1 \simeq \theta_2$. Denoting by (x_1, y_1), (x_2, y_2) the cartesian co-ordinates of the impact points of the two electrons in the plane of the SMD, and L the distance from the target to the SMD plane, the opening angle θ is given by:

$$\theta \equiv \frac{\sqrt{(x_1 - x_2)^2 + (y_1 - y_2)^2}}{L} = \frac{l}{L} \tag{5}$$

For two body kinematics with the target electron at rest, and the beam perpendicular to the SMD plane then $\theta = \theta_0$ where θ_0 is defined in Eqn.(2). Two different determinations of $E_{\rm beam}$, with very different systematic errors, are possible, depending on how the value of κ in Eqn.(1) is measured:

$$E_{\rm beam} = E_A : \qquad \kappa_A \equiv \frac{E_1 - E_2}{E_1 + E_2} \tag{6}$$

$$E_{\rm beam} = E_B : \qquad \kappa_B \equiv \frac{\tan\theta_1 - \tan\theta_2}{\theta} \tag{7}$$

where E_1 and E_2 are the energy of the electrons measured by the ECAL [7], and

$$\tan\theta_i \equiv \frac{\sqrt{(x_i - x_0)^2 + (y_i - y_0)^2}}{L} = \frac{l_i}{L} \qquad (i = 1, 2) \tag{8}$$

where (x_0, y_0) is the position of the beam in the SMD coordinate system. E_A is determined by information from both the SMD and the ECAL but is independent of the transverse beam position, whereas E_B uses only the SMD measurement but requires the transverse beam position to be known.

To study the precision required for the measured quantities θ, κ_A, κ_B it may be noted that from Eqn.(1):

$$\frac{SE_{\rm beam}}{E_{\rm beam}} = -2\frac{S\theta}{\theta} + 2\kappa_{obs} \cdot S\kappa - (S\kappa)^2 \tag{9}$$

here κ_{obs} is the measured κ (κ_A or κ_B); $\kappa_{obs} = \kappa + S\kappa$. In this equation and subsequently SX denotes the *shift* of the quantity X due to some systematic effect. The *precision*, ΔX with which X can then be measured depends on how accurately SX can be estimated. Since $S\kappa$ is typically much larger than $S\theta$, Eqn.(9) is written to first order in $S\theta$, and to second order in $S\kappa$. In general SX depends on some measurable or calculable parameters, for example the mean Fermi momentum of the target electron in the hydrogen atom, the beam size or the resolution of the ECAL. The aim of the simulations presented in Section 3 below is to calculate SX in terms of these parameters. Eqn.(9) indicates that to obtain a precision of 1 MeV on $E_{\rm beam}$ at 90 GeV requires that θ should be known to 5 parts in 10^6. If $L = 30$ m, the required tolerance

[7] this definition and the exact definition in (4) differs only by a factor $(1 + 10^{-5})$ when $E_{\rm beam} = 90$ GeV

on l, the distance between the SMD hits of two electrons, is 1 μm compared to the typical size of $l = 20$ cm (corresponding to the minimum θ) and on L is 150 μm. This level of survey accuracy is not unrealistic. Since the Møller detector is cross-calibrated relative to the RDP measurement the absolute values of L and l are not required to be known. They must however remain constant within the specified tolerances between cross-calibrations. It should be noted that, compared to this absolute accuracy, the requirement on the resolution of l is much looser. The beam energy has an intrinsic spread of $\sigma_E/E = 1.5 \times 10^{-3}$, (hence $\sigma_l/l = 0.75 \times 10^{-3}$). There is an effect of similar magnitude from the Fermi motion of the target electrons. Thus the position resolution of the SMD should be about 50 μm, which can easily be achieved using standard silicon microstrip detector technology. From the definition in Eqn.(5) the opening angle θ is independent of the transverse position of the beam relative to the SMD. It depends only weakly on the angle between the beam direction and the detector axis (beam tilt and beam angular divergence), and the error on θ due to this effect is negligibly small. This is why θ is used in Eqn.(7) instead of the more obvious choice $\theta_0 = \tan\theta_1 + \tan\theta_2$ as in Eqn.(3). As shown in Section 4 below, the stability of L can be controlled to a fraction of a millimetre by observing ep scattering events.

The effect of $S\kappa$ is more complicated. The third term in (9), which is quadratic in κ, does not average to zero. The finite resolution of the κ measurement therefore causes a shift of the reconstructed beam energy by:

$$\overline{SE/E} \simeq -\overline{S\kappa^2}. \tag{10}$$

The second term which is linear to $S\kappa$ may average to zero if there is no correlation between $S\kappa$ and κ_{obs}. However, it depends on how the quantity κ is measured and how the underlying effects propagate. This will be studied in detail using Monte Carlo simulation in the next section. It should be pointed out that by restricting $|\kappa_{obs}|$ used in the analysis, the contribution from the second term can be reduced, but at the cost of event statistics.

The major contributions to $S\kappa$ are different for E_A and E_B. In the ECAL method, E_A,the finite energy resolution of ECAL and the gain calibration error are the dominant sources. In E_B the finite beam size and uncertainty in the beam position, with respect to which the electron scattering angle is measured (Eqn.(8)), are the most important.

Finally in this Section the statistical error of the $E_{\rm beam}$ measurement is estimated. The cross sections for Møller (e^-e^-) and Bhabha (e^+e^-) scattering, integrated over the angular range $-c_0 < \cos\theta^* < c_0$, where $\cos\theta^*$ is the scattering angle in the CM frame, are:

$$\sigma = \frac{4\pi\alpha^2}{s}\frac{c_0(9-c_0^2)}{(1-c_0^2)} \quad (\text{ Møller }) \tag{11}$$

$$\sigma = \frac{\pi\alpha^2}{s}\left\{8\left[\frac{2c_0}{(1-c_0^2)} + \ln\left(\frac{1-c_0}{1+c_0}\right)\right] + 9c_0 - \frac{c_0^3}{3}\right\} \quad (\text{ Bhabha }) \tag{12}$$

$\sqrt{s}$ is the total CM enegy of the scattering process (303 MeV at $E_0 = 90$ GeV). A minimum accepted scattering angle of 2 mrad in the lab. frame, corresponds to the centre of mass acceptance cut: $c_0 = 0.479$ at $E_0 = 90$ GeV. Where E_0 is the mean beam energy. The accepted Møller (Bhabha) cross sections are 15.5 (4.2) μb. With a luminosity (of the LEP beam on the target electrons) of $4 \times 10^{31}\text{cm}^{-2}\text{sec}^{-1}$ [6] the Møller (Bhabha) event rates are 620 (167) events per second. Thus in 2 hours 4.5×10^6 (1.2×10^6) of Møller (Bhabha) events will be collected. The statistical accuracy of the $E_{\rm beam}$ measurement is then determined by the spread on the

reconstructed E_{beam} distribution. The dominant contributions to the spread are due to the Fermi motion of the target electrons ($\sigma_E = 290$ MeV at $E_0 = 90$ GeV) and the energy spread of the LEP beam ($\sigma_E = 145$ MeV at $E_0 = 90$ GeV). The RMS spread of the E_{beam} distribution is found, in the Monte Carlo simulation described below to be $\sigma_E = 390$ MeV. For N recorded events the statistical error on the mean beam energy is:

$$\Delta E_0^{stat} = \frac{\sigma_E}{\sqrt{N}} = \frac{390\text{MeV}}{\sqrt{N}} \tag{13}$$

So, in 2 hours:

$$\Delta E_0^{stat} = 0.18\text{MeV} \quad (\text{ Møller }) \tag{14}$$

$$\Delta E_0^{stat} = 0.36\text{MeV} \quad (\text{ Bhabha }) \tag{15}$$

The statistical error is thus sufficiently small compared to the goal of 1-2 MeV overall accuracy.

3 Simulation of Systematic Effects

In order to assess the systematic effects, a Monte Carlo study was made with realistic assumptions. Radiative corrections, Fermi motion, beam energy spread, beam size, beam angular divergence and ECAL resolution were considered. The effect of each individual contribution was studied. The parameters of our model detector are:

L	:	30 m		
SMD acceptance	:	2.00 – 6.00 mrad		
ECAL acceptance	:	1.67 – 6.33 mrad		
ECAL resolution	:	$\sigma_E/E = 3.37/E(\text{GeV})^{1/4}$ %		
Beam size	:	$\sigma_x = 1.54$	$\sigma_y = 0.34$	(mm)
Divergence	:	$\sigma_{x'} = 28.5$	$\sigma_{y'} = 5.0$	μrad
Energy spread	:	$\sigma_E = 145$ MeV	(At $E_0 = 90$ GeV)	

In the simulation of the ECAL response, the energies of the photons (produced by radiation from electrons) were added to those of the nearest electron if they are separated from it, in the transverse plane, by less than 1cm at the ECAL position. The energy was then smeared with Gaussian distribution to simulate the energy resolution. All of these effects were incorporated in a Monte Carlo event generator. The results presented below used a modified version of the Bhabha event generator BHAGENE3 [9].

3.1 Radiative Corrections

The effects of photon radiation, (Fig.2) were investigated using three independent computer codes. In the first, following Ref.[6], 'effective photons' of energy E_γ were radiated collinear to each incoming or outgoing electron with the differential probability :

$$\frac{dP}{dx} = \beta x^{\beta-1} \tag{16}$$

where

$$\beta = \frac{\alpha}{\pi}[\ln(\frac{s}{m_e^2}) - 1], \quad x = 2E_\gamma/\sqrt{s}$$

The second code used is the Standard Model Bhabha scattering generator BHAGENE3 [9] with a suitably re-weighted angular distribution.[8] In this program up to two initial state and three final state photons are generated using an improved soft photon approximation in the full angular phase space. Mass effects in the near collinear region are explicitly taken into account. The shifts and smearing of the energy distributions were cross-checked using a third independent code BMOLLR [10], an $O(\alpha)$ exponentiated Monte Carlo generator for $e^-e^- \to e^-e^- + n\gamma$ where n may take any value.

The main effects of photon radiation are the following:

- Initial state radiation. Collinear photons radiated from the incoming beam or the target electron are not observed in the detector so $E_{vis} < E_{\rm beam}$. The Lorentz boost between the e^-e^- CM system and the LAB depends on the photon energy so that Eqn(1) is no longer valid. Non collinear initial state photons result in a non-zero angle between the plane defined by the scattered electrons and the beam direction. Thus $\theta \neq \theta_0$.
- Final state radiation. Collinear radiation does not effect the validity of Eqn.(1). Also, since such photons are detected in the ECAL, together with the scattered electrons they do not effect the calorimetric measurement of E_1, E_2. Non collinear photons will however modify Eqn.(1) in a similar way to non collinear initial state photons. They may also be outside the ECAL acceptance and so will modify the measured values of E_1 or E_2.

The energies of the detected photons were added to those of the nearest scattered electron to determine E_1, E_2. Figs.(3a,3b) show results from BHAGENE3 for E_A and E_B. For E_A calorimeter resolution effects (see below) are set to zero. The main effect is a loss of statistics from the narrow central peaks, due to highly radiative events rather than a significant increase in the width of this peak. It can be seen from Fig.3 that the migration of events from the central peak is much more severe for E_B than for E_A.

3.2 Binding Effects

The kinematical effects due to atomic binding of the target electrons are similar to those produced by initial state radiation in that the e^-e^- CM energy and the Lorentz boost between the e^-e^- CM and the Lab systems are modified. If a bound electron has Fermi momentum p_f then the CM energy $\sqrt{s}$ is modified according to the relation:

$$s' = s[1 - \frac{p_f}{m_e}\cos\chi] \tag{17}$$

where χ is the angle between $\vec{p}_f$ and the beam direction. In a GJT the hydrogen is actually in the form of 'clusters' of some 10^6 hydrogen atoms. Here the simplifying assumption is made

[8]This program, written for use at LEP1 energies also includes full one-loop electroweak corrections for s and t channel Z exchange. In this study it was used unmodified at $\sqrt{s} = 200 - 300$ MeV.

that the binding effects are the same as in atomic hydrogen. The distribution of p_f is given by the momentum wave function $\Psi(p_f)$ of the electrons in the ground state of the hydrogen atom. $\Psi(p_f)$ is calculated by taking the 3-dimensional Fourier transform of the radial wave function:

$$R_0(r) = (\frac{1}{a_0})^{\frac{3}{2}} 2e^{-\frac{r}{a_0}} \tag{18}$$

where a_0 is the Bohr radius ($= 0.529\mathring{A}$). The result is:

$$\Psi(p_f) = \frac{1}{[1 + (a_0 p_f)^2]^2} \tag{19}$$

So the probability distribution for p_f is:

$$\frac{dP}{dp_f} = 4\pi \left|\Psi(p_f)\right|^2 p_f^2 = 4\pi \frac{p_f^2}{[1 + (p_f/p_f^0)^2]^4} \tag{20}$$

where $p_f^0 = 1/a_0 = 3.73$ keV.

The modification of the centre of mass energy $\sqrt{s}$ to $\sqrt{s'}$ causes the opening angle θ to be modified according to $\delta\theta/\theta = (p_f/m_e) \cdot \cos\chi$. For a typical value of $p_f = p_f^0$ and $\cos\chi = \pm 1$, the shift of $\delta E_{\text{beam}}/E_{\text{beam}} = \pm 3.6 \times 10^{-3}$. It causes a significant increase in the width of the reconstructed E_{beam} distribution (larger than the LEP energy spread). However, this shift averages to zero when integrated over $\cos\chi$ and the net shift (due to higher order terms) is small. E_A, E_B distributions, including the effects of Fermi motion simulated according to Eqn.(20) are shown in Figs.(4a,4b) respectively.

3.3 Beam Size and Divergence

In the E_B method the parameter κ is defined by Eqns. (7) and (8). The main sources of $S\kappa$ are the uncertainties in the beam position and the finite transverse beam size. In the worst case, when the scattering plane is horizontal, and the collision point is also displaced horizontally from its mean position, the RMS of the collision point distribution is 1.54 mm. This corresponds to the shift in κ of 0.015 RMS. From Eqn.(10), the shift in the measured E_0 is estimated to be 20 MeV when $E_0 = 90$ GeV. In order to make a correction for this shift to an accuracy of 1 MeV, the beam size should be known to a level of 5% relative precision. Possible ways to achieve this precision are discussed in Section 4. The distributions of E_A, E_B including the effects of beam size, are shown in Figs.(5a,5b), and including the effects of beam divergence in Figs.(6a,6b).

3.4 ECAL Resolution and Gain Stability

In the E_A method, the ECAL resolution σ_E propagates to the resolution of κ_A (when $\kappa \simeq 0$) as $\sigma_\kappa = \sigma_E/\sqrt{2}E$. Similarly the relative gain calibration error between different calorimeter modules leads to a shift in κ. As indicated in Eqn.(10), a calorimeter with good energy resolution is important to reduce the contribution from $\overline{S\kappa^2}$. An energy resolution of $\approx 1\%$ has been

achieved at $E_e = 45$ GeV using existing techniques (crystal or lead glass calorimeters). Using such a calorimeter the shift due to the quadratic term in $S\kappa$ is about 4.5 MeV at $E_0 = 90$ GeV. To make a correction for this shift with an accuracy of 1 MeV, the ECAL resolution should be known to a relative accuracy of 10-20 %. The resolution can be continuously monitored using electrons from ep elastic scattering (see Section 4 below). The gain calibration can be maintained by using a suitable monitoring system. A precision of 0.1 % level for short/medium term has already been achieved in existing calorimeters [11]. The gain of the calorimeter can also be checked using the electrons from ep elastic scattering. Within the acceptance of the ECAL, the energy of the electron from this process is almost the full beam energy and varies only by 0.1 % over the range of accepted scattering angles. Thus the ECAL gain may be controlled at the level of $\simeq 0.1\%$. The effect of the ECAL resolution on E_A is shown in Fig.7.

3.5 A Simulation Results

The reconstructed E_{beam} for methods A, B with all effects considered are shown in Figs.(8a,8b). The systematic bias due to individual contributions as well as the overall systematic shift for both methods A and B, for $E_0 = 90, 50$ GeV are summarised in table 1. The shifts are estimated from the mean values of the corresponding distributions. For method A the most important

	$E_0 = 90$ GeV		$E_0 = 50$ GeV	
Parameter	E_A	E_B	E_A	E_B
Radiative effect	-0.2 ± 0.9	-0.03 ± 0.1	-0.1 ± 0.9	-0.05 ± 0.1
Fermi motion	-1.8 ± 0.3	-1.7 ± 0.3	-0.2 ± 0.1	-0.1 ± 0.1
Beam size	-0.2 ± 0.2	-8.8 ± 0.4	-0.06 ± 0.05	-0.8 ± 0.1
Beam divergence	-0.2 ± 0.2	-3.5 ± 0.2	0.06 ± 0.05	-0.2 ± 0.5
ECAL resolution	2.2 ± 0.30	–	0.3 ± 0.1	–
All effects	1.4 ± 0.4	-6.1 ± 0.4	2.2 ± 0.3	-2.9 ± 0.3

Table 1: Systematic shifts of the energy measurement $SE_i = \overline{E}_i - E_0$ in MeV (i=A,B) for $E_0 = 90$ GeV (column 2 and 3) and for $E_0 = 50$GeV (column 4 and 5). The errors quoted are statistical ($\sigma_{RMS}/\sqrt{N}$) for a sample of 2×10^6 events.

systematic shifts are due to ECAL resolution and Fermi motion, whereas for method B the finite beam size effect dominates. The results in Table 1 correspond to samples of 2×10^6 Monte Carlo events corresponding, for real data with a luminosity $4 \times 10^{31}\text{cm}^{-2}\text{sec}^{-1}$, to about one hour of data taking. The estimator used for the beam energy is, for both E_A and E_B, the mean of a truncated distribution $\overline{E}^{trun}$, to avoid sensitivity to the detailed form of the distribution. The truncation is done by using a symmetrical acceptance window centred at the nominal E_0 of width chosen such that 90 or 95 % of all events lie within the window. The entries in Table 1 correspond to a 90 % window. The stability of the procedure is illustrated in Table 2. and Fig.9 where $\overline{E}^{trun} - E_0$ is shown in the range $E_0 = 50$–90 GeV, and for the two different (90 % and 95 %) truncation windows. The changes in the mean energy for a different choice of window are $\simeq 1$ MeV for E_A and $\simeq 2$ MeV for E_B over the range of E_{beam} considered.

Attempts were made to find an empirical model defined by a few fixed parameters to describe the simulated E_A, E_B distributions. The most successful of these was a 5 parameter Breit-

Wigner plus Gaussian model with a common mean. However subtle changes in the shapes of the distributions as a function of $E_{\rm beam}$ rendered such fits unstable. [9] Although at 50 GeV consistent results were obtained between the mean energy parameter of the fit and $\overline{E}^{trun}$, this was no longer the case at higher energies, when either satisfactory fits could not be obtained, or a good fit was obtained but with a fitted mean value very different from both $\overline{E}^{trun}$ and the fitted mean values of neighbouring energy points.

E_0 (GeV)	50	60	70	80	90
Estimator					
$\overline{E}_A^{trun}$ (90 %)	2.2 ± 0.3	1.6 ± 0.4	0.4 ± 0.4	-0.3 ± 0.5	1.4 ± 0.4
$\overline{E}_A^{trun}$ (95 %)	2.4 ± 0.3	2.0 ± 0.4	1.6 ± 0.5	0.8 ± 0.6	1.2 ± 0.4
$\overline{E}_B^{trun}$ (90 %)	-2.9 ± 0.3	-7.3 ± 0.4	-7.9 ± 0.5	-7.5 ± 0.6	-6.1 ± 0.4
$\overline{E}_B^{trun}$ (95 %)	-5.2 ± 0.3	-8.1 ± 0.4	-10.1 ± 0.6	-9.1 ± 0.7	-7.9 ± 0.4

Table 2: Systematic shifts of the energy measurement $\overline{E}^{trun} - E_0$ (in MeV) for different estimators and beam energies. The errors quoted are statistical for a sample of 2×10^6 events.

4 Calibration of Important Parameters

In this section, we discuss calibration methods for two important quantities: the distance L between the target to the SMD which determines the accuracy of θ, and the transverse beam size and position relevant for the E_B method.

4.1 Monitoring the Target-Detector Distance using Elastic e-p Scattering

As mentioned in Section 2, a 1 MeV uncertainty on $E_{\rm beam}$ corresponds to a relative uncertainty in θ of 5 parts in 10^6. This implies, from Eqn.(5), that the distance L from the luminous region of the target to the detector plane must be controlled to the same accuracy, i.e. to a tolerance of ± 150 μm for $L = 30$ m. The gas jet has a dimension of several mm along the beam direction and its position and the size may not be stable. It is therefore proposed to monitor continuously the mean value of L, $(\overline{L})$ by detecting and analysing elastic e-p scattering events.

From two body kinematics, the scattering angles of electron and proton, $\theta_{\rm e}$ and $\theta_{\rm p}$ respectively, are related by the formula:

$$\tan\theta_{\rm p} = \frac{2}{\theta_{\rm e}(1 + E_{\rm beam}/m_{\rm p})} \tag{21}$$

[9] The problem of defining a stable estimator of the beam energy had not been fully solved when perliminary results of this study were presented in Ref.[4]. This explains the differences between the results shown in Ref.[4] and those given in Table 1.

For the SMD acceptance region: $2 < \theta_e < 7$ mrad and $50 < E_{\rm beam} < 90$ GeV, θ_p is limited to the range: $71° < \theta_p < 87°$. The recoil proton is detected, in coincidence with the scattered electron, in the RPD, a small silicon strip detector *in vacuo*, built into the support of the GJT. A similar arrangement was used in the UA6 experiment [8]. If r is the radial distance of the e-p collision point from the RPD and, z and z_D are the coordinates, parallel to the beam direction, of the collision point and the proton hit in the RPD respectively, then the z coordinate of the collision point is determined to be:

$$z = z_D - \frac{r\theta_e}{2}(1 + \frac{E_{\rm beam}}{m_p}) \tag{22}$$

If d_e is the transverse distance from the plane of the RPD of the electron hit in the SMD, then $\theta_e = (d_e - r)/L$. The error on z is given by:

$$\delta z = \delta z_D - \frac{1}{2L}(1 + \frac{E_{\rm beam}}{m_p})[r\delta d_e + \delta r(d_e - 2r)] - \frac{r(d_e - r)}{2L}\frac{\delta E_{\rm beam}}{m_p} \tag{23}$$

Assuming $r = 10$ cm, $\theta_e = 3$ mrad, the contribution from the third term is negligible ($\simeq 30\mu$m even if $\delta E_{\rm beam}$ is as big as 200 MeV). The dominant contribution from the second term is the δr from the transverse beam size. In the worst case where the scattering plane is horizontal, $\delta r \simeq 1.5$ mm, giving $\delta z = 250\mu$m. Because of this large contribution to δz from the uncertainty in r only a modest spatial resolution of $\delta z_D \simeq 100\mu$m is adequate for the RPD. Thus, on an event-by-event basis, z can be measured with a precision of a fraction of a millimetre. The accuracy with which the mean value of z for an ensemble of events can be determined is then completely dominated by the statistical error $\sigma_z^{targ}/\sqrt{N}$ where N is the number of recorded events and σ_z^{targ} is the length of the luminous region of the target, typically $\simeq 5$ mm.

Within an accuracy of $\simeq 10\%$ the observed cross section for e-p coincidence events is given by the Rutherford scattering formula:

$$\sigma(ep \rightarrow ep) = \frac{4\pi\alpha^2}{E_{beam}^2}(\frac{1}{\theta_{e,MIN}^2} - \frac{1}{\theta_{e,MAX}^2})A_\phi \tag{24}$$

where $\theta_{e,MIN}$ and $\theta_{e,MAX}$ are the minimum and maximum scattering angle of accepted electrons, and A_ϕ is the azimuthal acceptance. With $E_{\rm beam} = 90$ GeV, $\theta_{e,MIN} = 2$ mrad, $\theta_{e,MAX} = 7$ mrad and $A_\phi = 0.16$ (two microstrip detectors, back-to-back in ϕ of 5 cm width, at a distance of 10 cm from the beam line) Eqn.(24) gives $\sigma(\text{ep} \rightarrow \text{ep}) = 7.4\mu$b, or 296 events/second with a luminosity of 4×10^{31} cm^{-2}sec^{-1}. In one hour of data collection 1.1×10^6 events will be recorded and the mean longitudinal target position determined with a statistical accuracy of:

$$\frac{\sigma_z^{targ}}{\sqrt{N}} = \frac{5\text{mm}}{\sqrt{1.1 \times 10^6}} = 4.8\mu\text{m}$$

This is more than an order of magnitude better than the tolerance of $\pm 150\mu$m in $\overline{L}$ required for 1 MeV precision on $E_{\rm beam}$.

4.2 Monitoring the transverse beam profile using Møller events

Precise monitoring of the transverse beam size and position is important for the E_B method. Here we discuss ways to monitor them using the Møller events. The basic idea is that, since

the majority of the electron pairs are coplanar with the beam direction, in the transverse plane the vertex position of an event lies on a straight line between the positions of the electrons in the SMD plane (see Fig.(10)). Two methods are considered. The intersection of the line between the two hit positions of the electrons with the nominal Y-axis (X-axis) is, to a good approximation, the Y (X) coordinate of the vertex position if the line is nearly parallel to the X-axis (Y-axis). The X,Y beam profiles can be measured in this way. A merit of this method is that it allows a fast online monitoring. An example of Monte Carlo simulation of the reconstructed profiles is shown in Fig.(11). The tail of the distribution is due to acoplanar events caused by hard photon radiation.

The second method uses a maximum likelihood fit to a model of the distribution of the luminous region. The line joining the positions of the two electrons recorded in the SMD has a high probability of passing close to the mean beam position (Fig 12). The probability $\mathcal{P}$ to find two electrons in the SMD at (x_1, y_1) and (x_2, y_2) which are produced at (x, y) can be calculated event by event for a certain model of the beam profile function $B(x, y; x_0, y_0, \sigma_x, \sigma_y)$, where (x_0, y_0) and (σ_x, σ_y) are the position and spread of the beam respectively. For a given ensemble of Møller events, the likelihood $\ln \mathcal{L} = \sum \ln \mathcal{P}$ is maximised to obtain the beam parameters .

The two methods have been tested by Monte Carlo simulation. It is sufficient to collect 5000 Møller events to determine the horizontal beam size to a relative precision better than 5% and the mean beam position better than 100μm. This number of events can be collected in about 10 seconds. Hence the beam geometry can be monitored continuously several times per minute.

5 Conclusion

Two complementary methods, with different dominant systematic errors, to measure the LEP beam energy using Møller scattering have been presented. The calibration of all relevant parameters (calorimeter resolution and gain, beam size and position, target–detector distance) can be determined either directly from the Møller scattering data themselves, or from concurrently detected ep elastic scattering events. A statistical error of 1 MeV on the mean beam energy is obtainable in about 3 minutes of data taking time at 90 GeV beam energy. The measurement can be made during LEP physics runs, thus a continuous monitoring of the beam energy is possible. A detailed simulation taking into account all known systematic effects shows systematic shifts of $\leq$ 2 MeV, $\leq$ 10 MeV from the actual mean beam energy using E_A, E_B respectively, over the range $50 < E_{\rm beam}(\rm GeV) < 90$ (Fig 9). It should be noted that, in contrast to a previous similar study [6], binding effects on the electron target that give the dominant contribution to the energy smearing, have been taken into account. The precision of the beam energy measurement (since cross-calibration with RDP is performed at, say, 50 GeV) depends on the accuracy with which the change of the systematic shift with $E_{\rm beam}$ is simulated. If the simulation is accurate to $\pm$20%, then the corresponding error on $E_{\rm beam}$ from E_A is a fraction of an MeV, and from E_B is about 2 MeV.

An improved measurement of $E_{\rm beam}$ may have two effects on the M_W measurement at LEP2. Firstly, for a given integrated luminosity the error on M_W is reduced. Secondly less integrated luminosity is required to obtain a given accuracy on M_W. These effects are illustrated by

considering several different scenarios for the statistical and systematic errors. The following assumptions are made concerning these errors:

- $\Delta M_W^{stat} = 25$ MeV. Combined statistical error of four experiments each with an integrated luminosity of 500 pb^{-1} [5].
- $\Delta M_W^{TD} = 10$–35 MeV. Detector and theoretical systematic error [5].
- $\Delta M_W^{FL} = 9$–20 MeV. Systematic error from the beam energy uncertainty using the flux loop extrapolation method [4].
- $\Delta M_W^{MD} = 3$ MeV. Systematic error from the beam energy uncertainty using RDP with high energy extrapolation by the Møller technique. Contributions of 2 MeV (RDP and Møller), 2MeV (interaction point extrapolation) are added in quadrature.

These errors are assumed to be uncorrelated and added in quadrature to give the total error on M_W, ΔM_W^{tot}. Three scenarios are considered :

(I) In Table 3 ΔM_W^{tot} is shown as a function of ΔM_W^{TD} for the Møller and flux loop methods. Given between brackets beside the flux loop entries is the reduction factor in ΔM_W^{tot} given by the Møller method.

(II) If the flux loop method with 500 pb^{-1} of integrated luminosity is replaced by the Møller one the integrated luminosity required to obtain the same value of ΔM_W^{tot} is reduced by a factor 0.90 (0.61) for $\Delta M_W^{FL} = 9$ MeV (20 MeV). These reduction factors are independent of ΔM_W^{TD}.

(III) If the Møller method with 500 pb^{-1} of integrated luminosity is replaced by the flux loop one, then in order to obtain the same value of ΔM_W^{tot}, 565 pb^{-1} (1335 pb^{-1}) are required for $\Delta M_W^{FL} = 9$ MeV (20 MeV). These luminosities are independent of ΔM_W^{TD}.

ΔM_W^{TD} (MeV)	10	15	24	35
Møller	27.1	29.3	34.8	43.0
Flux Loop ($\Delta M_W^{FL} = 9$ MeV)	28.4 (0.95)	30.5 (0.96)	35.8 (0.97)	43.9 (0.98)
Flux Loop ($\Delta M_W^{FL} = 20$ MeV)	33.5 (0.81)	35.4 (0.83)	40.0 (0.87)	47.4 (0.91)

Table 3: Total errors on the W mass measurement (in MeV) and reduction factors (in brackets) if Møller replaces flux loop extrapolation

In summary, the impact of the Møller method is an improvement on the overall error of the W mass measurement that may vary from 2% to 20% depending on the actual values of ΔM_W^{TD} and ΔM_W^{FL}. In all cases the improvement on the error obtained using Møller scattering is equivalent to a reduction of the statistical error that would require a substantially larger integrated luminosity. The cost of the extra running time needed to obtain the latter is expected to be considerably in excess of the estimated $\simeq$ two million SF cost of the Møller detector.

Finally it may be remarked that the Møller scattering method described here, unlike RDP, can be used for precise energy measurements in one pass linear electron colliders.

Acknowledgements
We should like to thank M.Placidi for his continous encouragement of this work during the LEP2 study in 1995, and D. Schaile for her contributions in the early stages. Comments from M.Bourquin, M.N. Kienzle-Foccaci, F.Muheim and J.Wenninger have helped to improve the clarity of the presentation. Discussions with W.Kubischta about the gas jet target are also gratefully acknowledged.

References

[1] L.Arnaudon et al. Z. Phys. C66 (1995) 45.

[2] M.Placidi and R.Rossmanith, Nul. Inst. Meth. A274 (1989) 79.

[3] A.A.Sokolov and I.M.Ternov, Sov. Phys. Doklady Vol. 8 No.2 (1964) 1203.

[4] Report of the Working Group on Beam Energy Measurements at LEP in Proceedings of the LEP2 Study (Ed. G.Altarelli, T.Sjöstrand and F.Zwirner), CERN Yellow Report CERN 96-01 (Ed. G.Altarelli, T.Sjöstrand and F.Zwirner) Vol.1 P59.

[5] Report of the Working Group W Mass Measurements in Proceedings of the LEP2 Study (Ed. G.Altarelli, T.Sjöstrand and F.Zwirner), CERN Yellow Report CERN 96-01 (Ed. G.Altarelli, T.Sjöstrand and F.Zwirner) Vol.1 P141.

[6] P. Galumian et al., Nucl. Instrum. and Meth. A327 (1993) 269.

[7] A.Blondel in 'Precision Tests of the Standard Electroweak Model', Ed. P.Langacker. World Scientific 1995, P277.

[8] J.Antille et al., Phys. Lett. B194 (1987) 568.

[9] J.H.Field, Phys. Lett. B323 (1994) 423; J.H.Field and T.Riemann Comp. Phys. Comm. 94 (1966) 53.

[10] S.Jadach and B.F.L. Ward, UTHEP-94-0702 July 94.

[11] OPAL collaboration, Nucl. Instrum. and Meth. A305 (1991) 275; L3 Collaboration, A.Bay et al., Nucl. Instrum. and Meth. A32 (1991) 119.

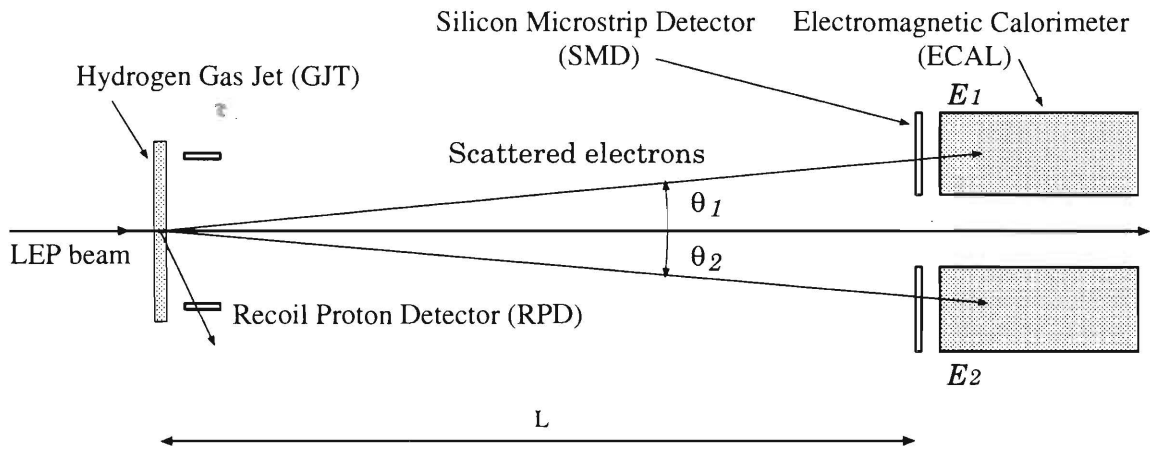

Figure 1: The Møller detector.

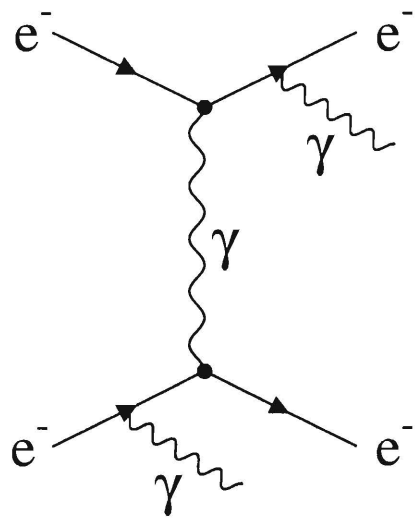

Figure 2: Møller scattering diagram with initial and final state radiation.

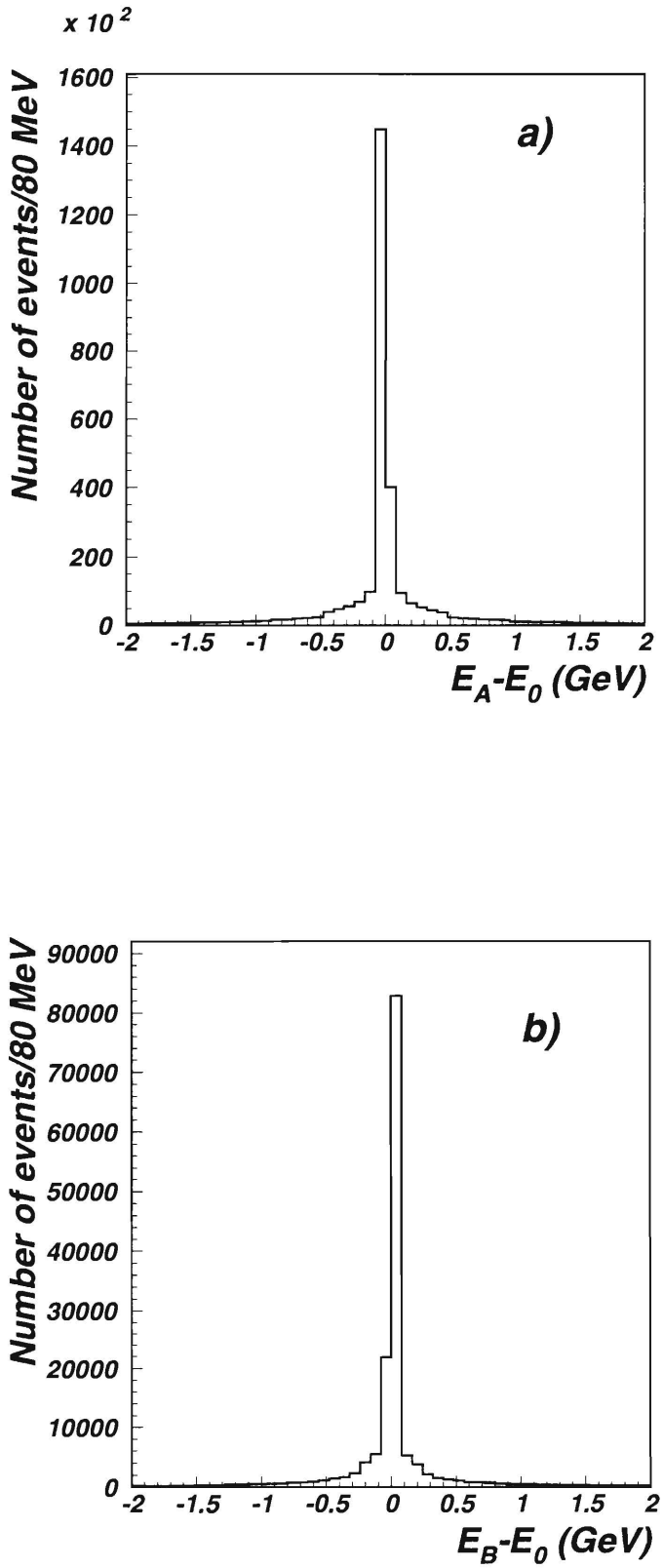

Figure 3: Effect of radiative corrections on a) E_A, b) E_B. ($E_0 = 90$ GeV)

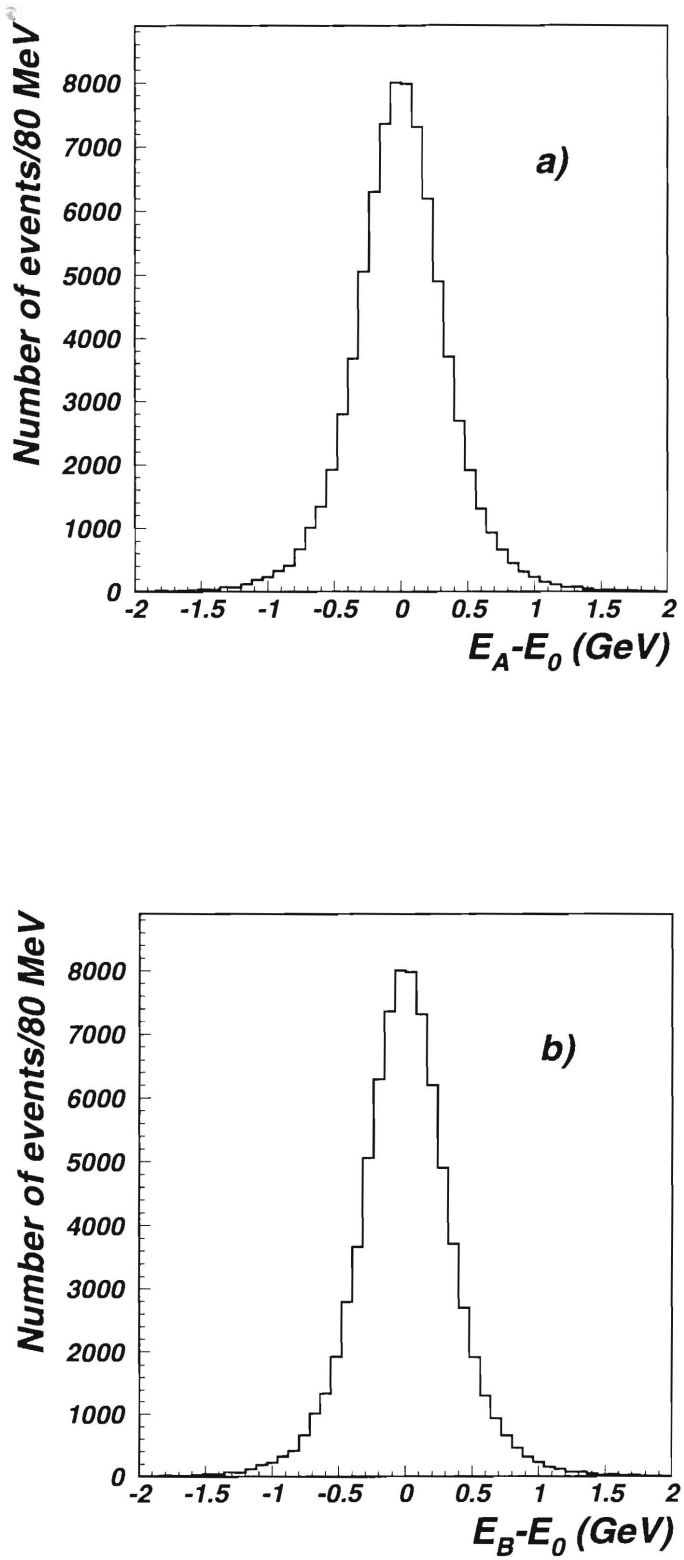

Figure 4: Effect of binding corrections on a) E_A, b) E_B. ($E_0 = 90$ GeV)

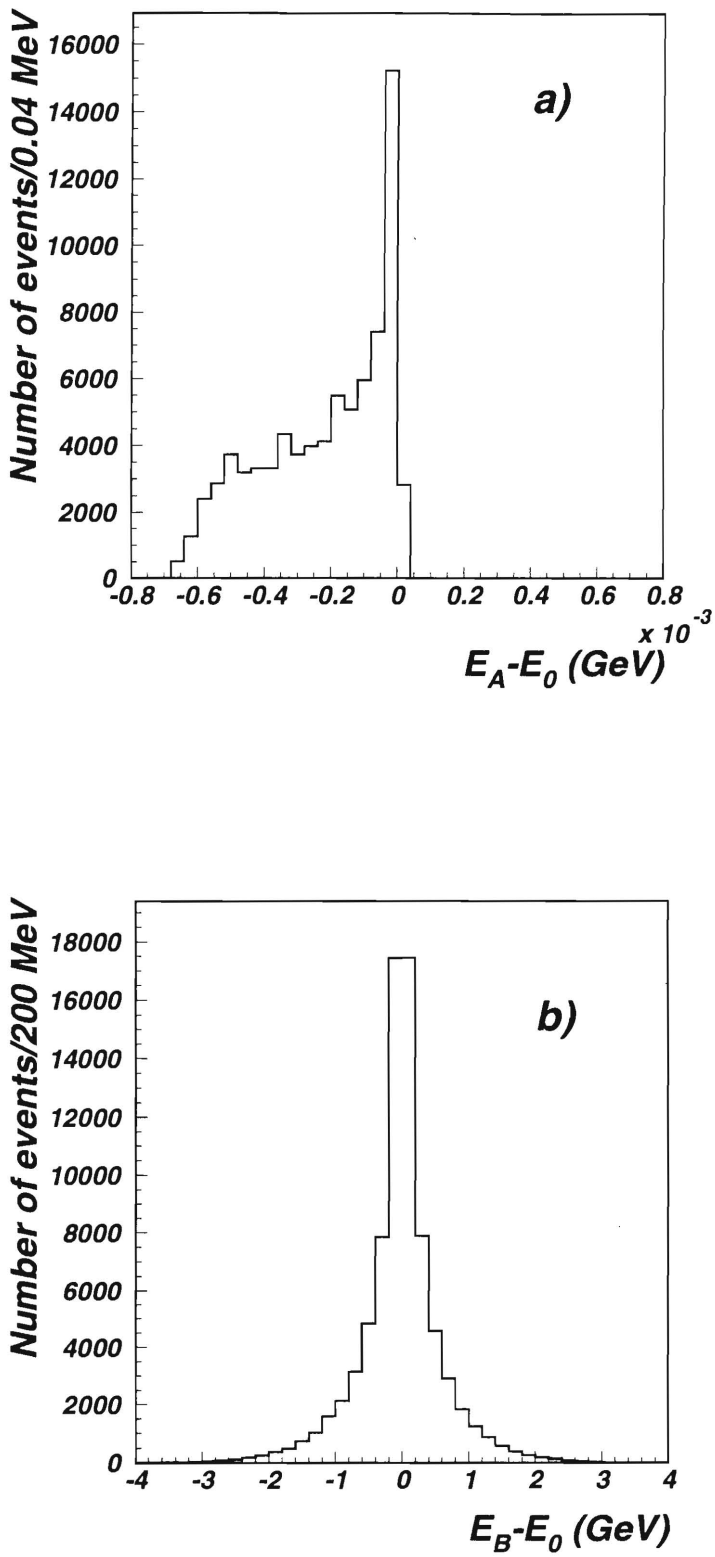

Figure 5: Effect of transverse beam size on a) E_A, b) E_B. ($E_0 = 90$ GeV)

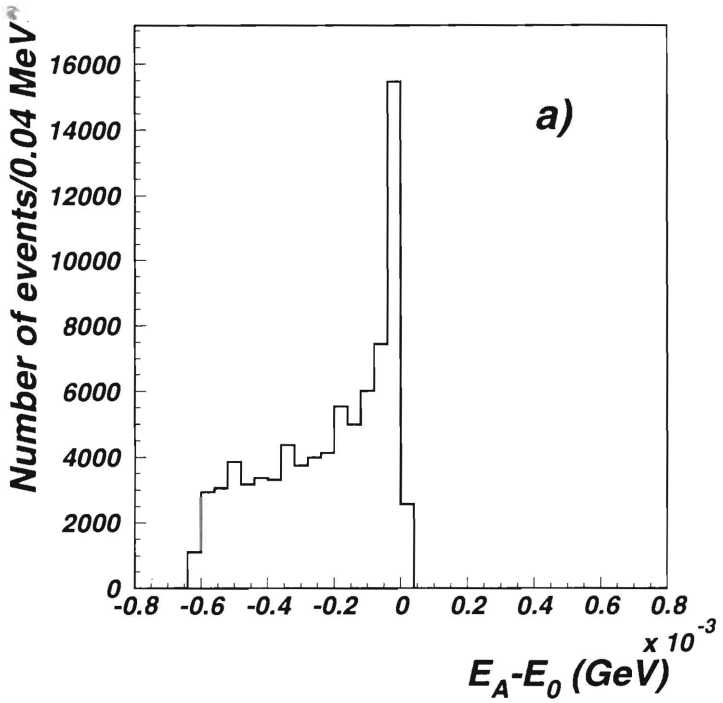

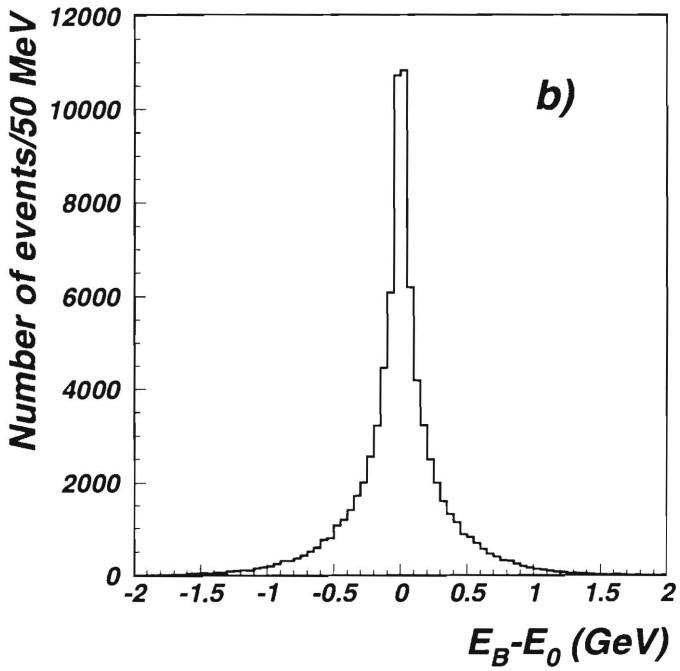

Figure 6: Effect of beam divergence on a) E_A, b) E_B. ($E_0 = 90$ GeV)

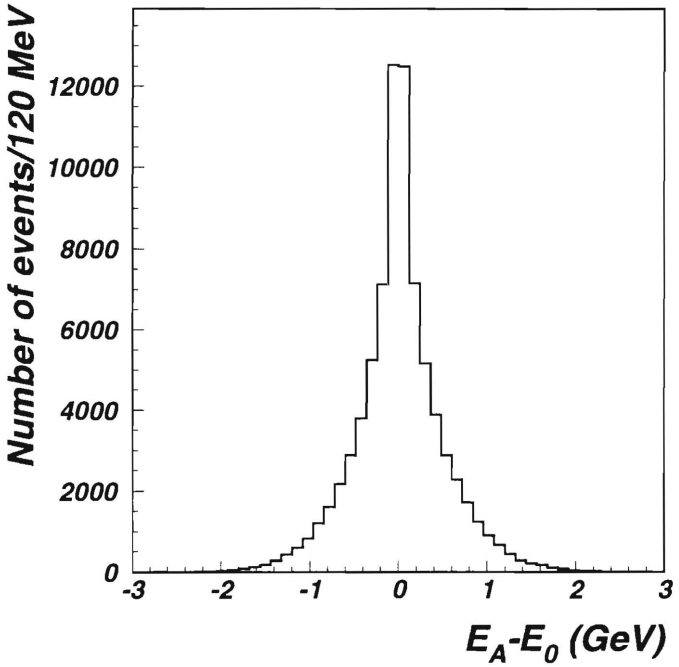

Figure 7: Effect of calorimeter resolution on E_A.($E_0 = 90$ GeV)

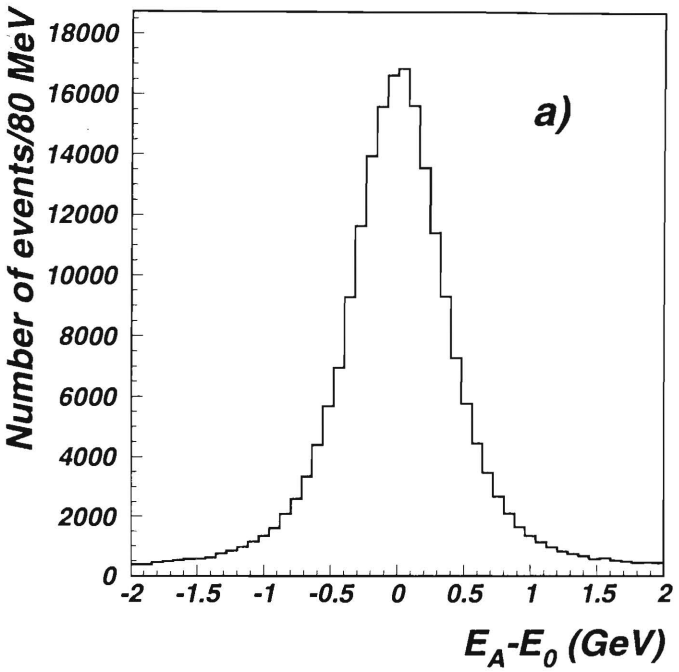

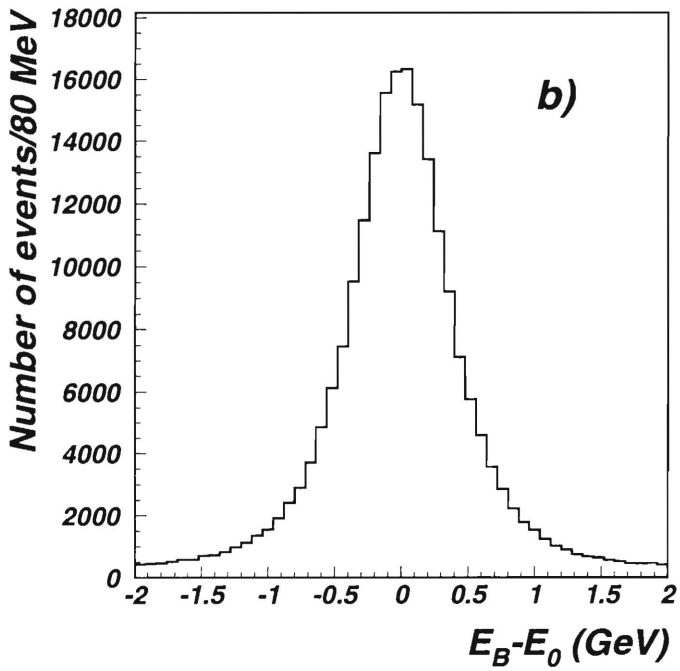

Figure 8: Effect of all corrections on a) E_A, b) E_B. ($E_0 = 90$ GeV)

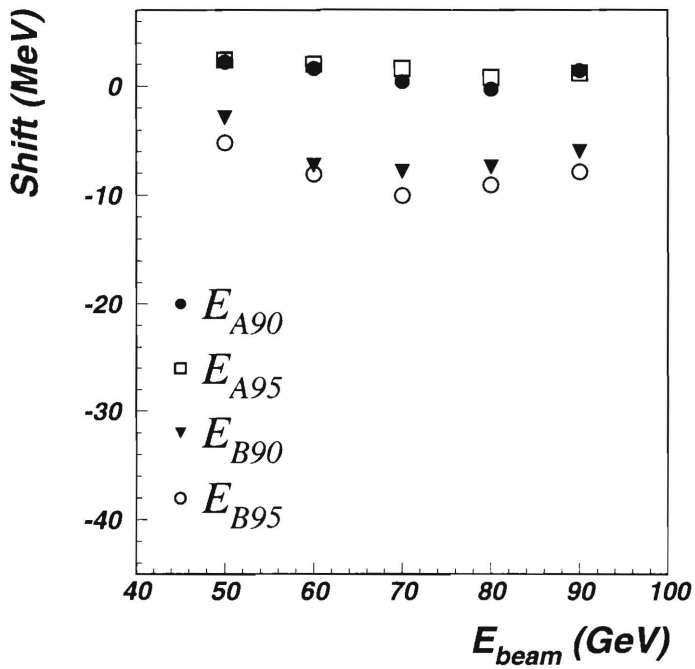

Figure 9: Energy shifts of E_A and E_B as a function of the beam energy.

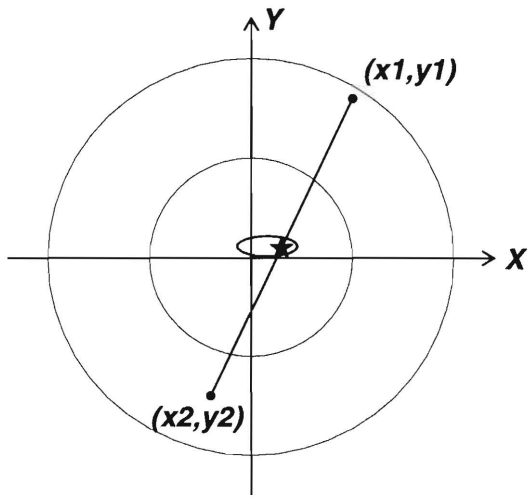

Figure 10: Beam profile and Møller event.(Transverse View).

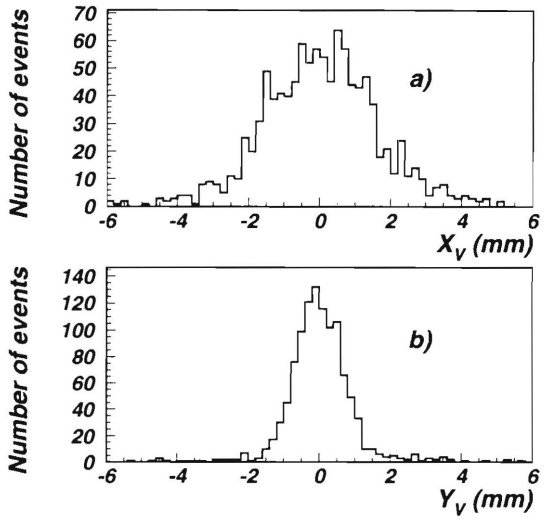

Figure 11: The reconstructed beam profile : (a) X-projection and (b) Y-projection.

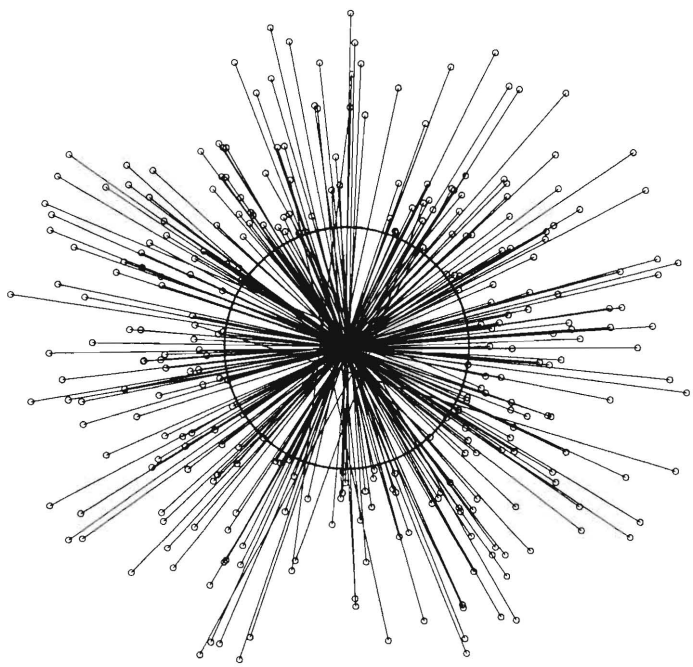

Figure 12: Distribution of lines joining the two electron hits in the SMD in simulated Møller events. (Transverse View).